Incorporating Copper to Biodegradable Magnesium Alloy Vascular Stents via a Cu(II)-Eluting Coating for Synergistic Enhancement in Prolonged Durability and Rapid Re-Endothelialization

Ling-Yu Li, Zhou Yang, Xiang-Xiang Pan, Bo-Xuan Feng, Rui Yue, Bo Yu, Yu-Feng Zheng, Jin-Yun Tan,* Guang-Yin Yuan,* and Jia Pei*

Biodegradable magnesium-based scaffolds present outstanding potential to revolutionize the treatment of coronary artery diseases, in which full recovery of arteries without long-term irritation of implants is anticipated for averting adverse events associated with the permanent stents. However, overfast degradation of magnesium (Mg) alloys obstructs their extensive applications in terms of early structural failure and impaired biocompatibility. Herein, a facile copper-incorporated coating system through nonaqueous phase synthesis of polydopamine is developed to facilitate Cu(II) capture along with robust film deposited on easily corrodible Mg, which subsequently enables sustained Cu(II) elution. It remarkably enhances corrosion resistance and impedes Mg degradation, which also contributes to improved, superior cytocompatibility, and abolished hemolysis. Moreover, through simultaneous control of Cu(II) and Mg(II) release to modulate the local microenvironment, a synergistic biochemical effect on desirable vascular cell selectivity is triggered for boosted endothelial cell viability and suppressed smooth muscle cell. Stent implantation into rabbit abdominal aorta thus exhibits accelerated re-endothelialization completed in a week, and enhanced biological outcomes, alleviated complications and prolonged structural durability in 3-month follow-up. Collectively, this work opens up an alternative route of deploying a multifunctional surface modification strategy tailoring active interplay with the Mg matrix for better outcomes of next-generation bioresorbable vascular stents.

1. Introduction

Coronary artery disease (CAD) is considered as a major public health threat with high morbidity, particularly in the current

prevalence of global aging. For decades percutaneous coronary intervention combined with the use of bare-metal stents (BMS) or drug-eluting stents (DES) has become the most prevalent clinical method for the noninvasive treatment of CAD.[1,2] However, BMS stenting is often evidenced with a high risk of in-stent restenosis (ISR) and thrombosis, predominately due to excessive neointimal formation and inflammation. In an attempt to alleviate restenosis, DES is integrated with antiproliferative drugs to suppress vascular smooth muscle cells (VSMCs), whereas the long-term success is shattered by the elevated late ISR and complications associated with delayed re-endothelialization and permanent, rigid caging. $^{[3-5]}$ To address such a cascade of critical clinical problems which even bring on catastrophic consequences, researchers have lately sought to explore a new horizon with development of next-generation fully bioresorbable scaffolds (BRS). Through liberating the coronary arteries from permanent stenting with foreign materials, BRS thus possesses potential to restore normal morphology and physiology of the

vessels, obviating long-term limitations of conventional stents and possibly conveying additional benefits.^[6]

In light of its innate merits of great biosafety, mechanical compliance, and biodegradability, magnesium and its alloys

L.-Y. Li, X.-X. Pan, B.-X. Feng, R. Yue, G.-Y. Yuan, J. Pei
National Engineering Research Center of Light Alloy Net Forming
and State Key Laboratory of Metal Matrix Composite
School of Materials Science and Engineering
Shanghai Jiao Tong University
Shanghai 200240, China
E-mail: gyyuan@sjtu.edu.cn; jpei@sjtu.edu.cn
Z. Yang, B. Yu, J.-Y. Tan
Shanghai Key Laboratory of Vascular Lesions Regulation and Remodeling
Shanghai 200444, China

The ORCID identification number(s) for the author(s) of this article can be found under https://doi.org/10.1002/adfm.202205634.

DOI: 10.1002/adfm.202205634

B. Yu, J.-Y. Tan
Department of Vascular Surgery
Huashan Hospital
Fudan University
Shanghai 200040, China
E-mail: m.tan@fudan.edu.cn
Y.-F. Zheng
School of Materials Science and Engineering
Peking University
Beijing 100871, China
G.-Y. Yuan, J. Pei
Shanghai Innovation Institute for Materials
Shanghai 200444, China





www.afm-journal.de

(Mg) with temporary scaffolding capacity have recently emerged as a hotspot among diverse absorbable candidates of polymers and metals. In addition, the released magnesium ion (Mg²⁺, Mg(II)), as an integral element for the human body, is well recognized to play a pivotal role in regulating vascular tone, e.g., thrombosis, inflammation, proliferation, and migration of vascular endothelial cells (VECs) and VSMCs.[7] Nowadays, bioresorbable Mg-based cardiovascular stents still face tremendous technical challenges, particularly due to their aggressive corrosion and degradation feature in aqueous medium, leading to early structural failure prior to the accomplishment of its mission. On the other hand, excessive local release of Mg degradation products would also destruct vessel microenvironment and even induce risks of cytotoxicity, hemolysis, and other adverse events.^[8] Accordingly, substantial efforts, predominantly on the two approaches of alloying and surface modification, have been dedicated to improving the vulnerable corrosion resistance of Mg and eventually to coordinate the degradation behavior with biological response. A series of Mg alloys (AZ31,[9] WE43,[10] Mg-Nd-Zn-Zr,[8] Mg-Zn-Y-Nd,[11] etc.) have been successively developed in the past decade as potential biodegradable stent materials. Nonetheless, availability of alloying elements is enormously restrained by the load-bearing requirement, and more importantly, the high susceptibility to severe galvanic corrosion which instead aggravates Mg degradation and biocompatibility. As such, a large variety of metallic elements, e.g., Cu, Ca, and Fe, are known to be crucial for arterial tone regulation and vascular functions, thus may be unfavored with Mg alloying for adequate scaffolding life expectancy.^[6]

On the other hand, surface modification with functionalized coating is another feasible and essential method to provide corrosion protection for Mg, including chemical conversion layers and deposit coatings, e.g., fluoride, phosphate layer, sol-gel inorganic coating, organic self-assembly monolayers, and so on.[12] Nonetheless, achieving long-term effectiveness and the controllable corrosion rate is quite difficult for biomedical Mg alloys as implant materials. In previous study, the generation of a compact MgF2 conversion coating exhibited effective anticorrosion for only several days, but failed in prolonged protection in chloride-containing physiological environment.^[13] Furthermore, apart from tuning stents degradation, additional biofunction is particularly desirable for inhibiting ISR and other complications, possibly via appropriate regulation of blood cell response and vascular remodeling process. Among various surface treatments, polymer film is outstanding for tailoring versatile surface functionalities, which allows for further modification with drug delivery, immobilization of peptides, growth factors and even biocatalysts.^[14] At present, the most typical polymer-based coatings in use follow those established DES which were prepared through deposition of resorbable polyesters, loaded with antirestenosis/anti-inflammation agents, e.g., Sirolimus and Paclitaxel.^[15] However, regardless of permanent or degradable stents, an inevitable issue with DES lies in the impaired regeneration and dysfunctions of vascular endothelium due to the detrimental effects of the drug release. [16,17] It therefore poses a serious concern whether this conventional gold standard remains most suitable for the new-generation bioresorbable stents to harness their full potential as a promising breakthrough in this era. Alternatively, there is a recent

trend in designing bioactive polymer-based coating systems for generating more favorable interfacial microenvironment, albeit in its infancy for biodegradable Mg due to complexity in appropriate multifunctionality integration of balanced stent degradation and vascular remodeling. In particular, mussel-inspired polydopamine (PDA) coating is well reported for its universal good adherence and excellent biocompatibility, of which the performance is nevertheless highly dependent on polymerization, deposition and coating structure and stability.^[18–20] Traditional synthesis method via immersion in Tris-HCl aqueous solution containing dopamine (DA) was previously reported with obvious corrosion cracks generated on Mg-based substrates, thus hindering its further applications.^[21]

Herein, we proposed a facile and potent surface modification strategy for simultaneous tailoring of degradation and bioefficacy for Mg stents by constructing a robust copper-incorporated PDA top coating. In our case, compact, uniform PDA-based thin film with tunable thickness and varied Cu(II) content was successfully realized on corrodible Mg-based substrates, through a nonaqueous phase synthesis method by utilizing Cu(NO₃)₂/ammonia as reaction triggers. Meanwhile, Cu(NO₃)₂ feeding also enabled Cu(II) capture via coordination into the PDA network during polymerization and film deposition. Rather than accelerating galvanic corrosion as with the alloying approach, this coating integration of copper greatly augmented the corrosion resistance of Mg matrix in the long term. It thus allowed for retarded degradation with controlled release of Mg degradation products, and sustained, localized release of Cu(II) to orchestrate, reengineer the local microenvironment. Systematic in vitro and in vivo investigations unveiled a previously unknown synergistic role of Cu(II) together with Mg(II) in differential modulating cells response of VECs and VSMCs, hence the rapid re-endothelialization and amelioration of neointimal hyperplasia poststents implantation (Figure 1). Overall, the presented integration of PDA/Cu(II) coating system on Mg stents shows great promise to serve as a multifunctional biosurface to better leverage Mg degradation for prolonged stent durability and improved outcomes.

2. Results and Discussion

2.1. Surface Characterizations

As the conventional synthesis condition of PDA in aqueous solution containing Tris-HCl^[19] or other aggressive trigger agents^[18] rather deteriorated Mg corrosion and resulted in highly defective film with cracks and corrosion products, herein we employed a new synthesis approach with DA in ethanol solvent conditioned with a stronger alkali of ammonia, and Cu(NO₃)₂ as cotrigger and reactant. The Cu(II)-integrated coating system was fabricated on a previously reported Mg-Nd-Zn-Zr^[8] alloy (Jiao Da Bio-Mg, denoted as JDBM) as a candidate stent material, through a simple dipping process of sequential stacking of pure PDA layer as pretreatment followed by an ultrathin PDA/Cu(II) outermost coating. To reveal the impact of copper incorporation in the subsequent coating performance, different feeding amount of Cu(NO₃)₂ (namely, Cu5, Cu10, and Cu20) was respectively added during the reaction, generating

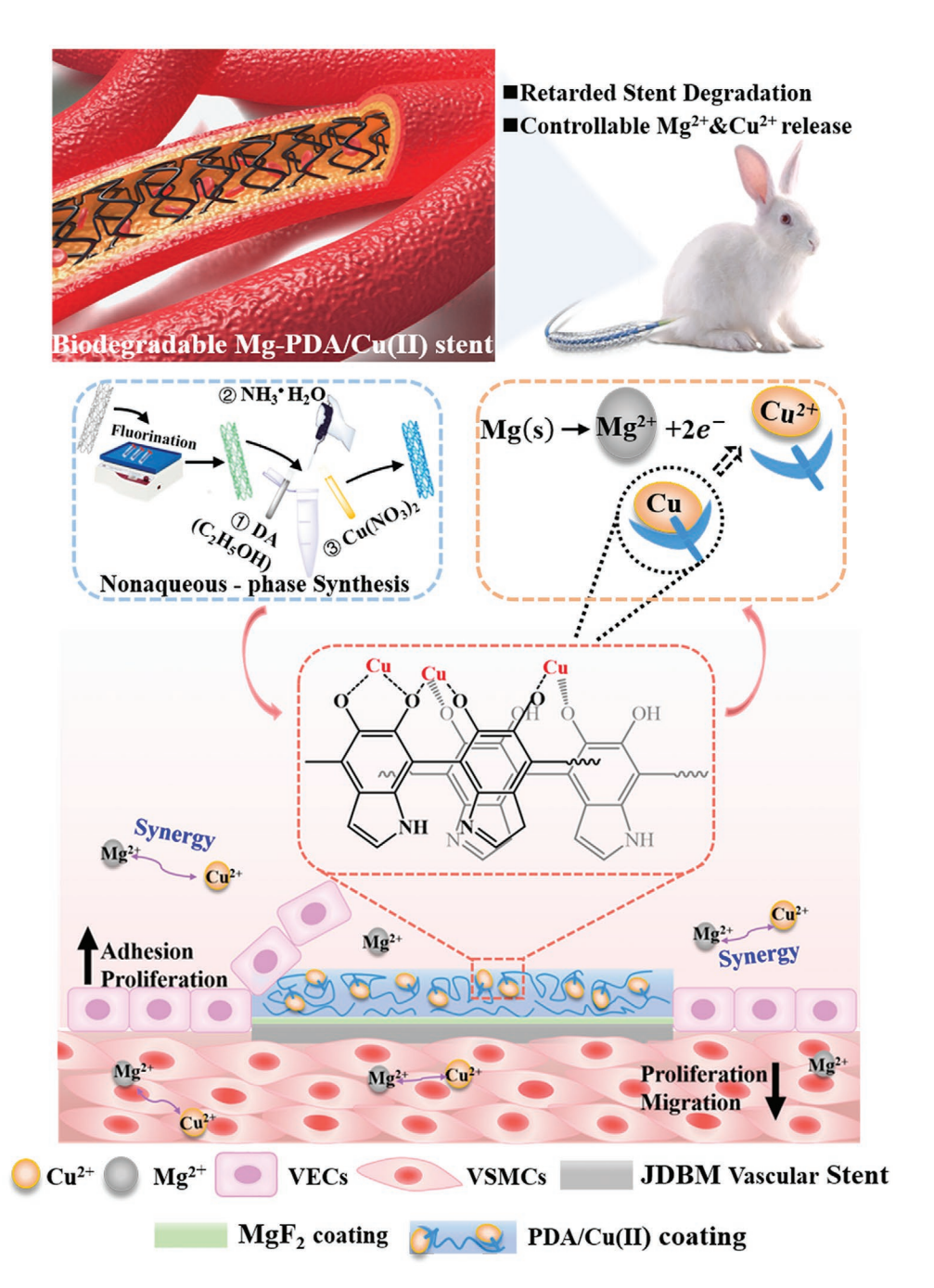


Figure 1. Schematic illustration of PDA/Cu(II) eluting coating on Mg-based cardiovascular stents for controlling Mg matrix degradation and modulating local release of Mg(II) and Cu(II), which contributes to superior bioefficacy with prolonged stent durability, and enhanced anti-inflammation and antirestenosis functions through synergistic effect on fostering VECs while inhibiting VSMCs.

self-assembly polymeric film containing varied copper content on Mg surface. The resultant sample surface morphologies and corresponding water contact angles (WCA) of PDA and PDA/Cu(II) coatings were depicted in Figure 2A. As compared to the bare substrate of superhydrophilicity (WCA < 5°), PDA, Cu5, Cu10, and Cu20 coatings all displayed elevated hydrophobicity with similar WCA ranging 47–52° (Table S1, Supporting Information). In scanning electron microscopy (SEM) examination, all these samples except Cu 20 exhibited a uniform and

nonporous coating structure with a number of nanoparticles evenly distributed, which were typical polymerization aggregates as reported with single PDA prepared in aqueous solution, presumably attributable to the rapid polymerization of DA and homogenous nucleation followed by the quick deposition of PDA nanoparticles. [18] In contrast, Cu20 group was evidenced with cracks on the entire surface, suggesting high feeding concentration of Cu(NO₃)₂ might be detrimental to the compact coating structure, which probably initiated the dissolution of

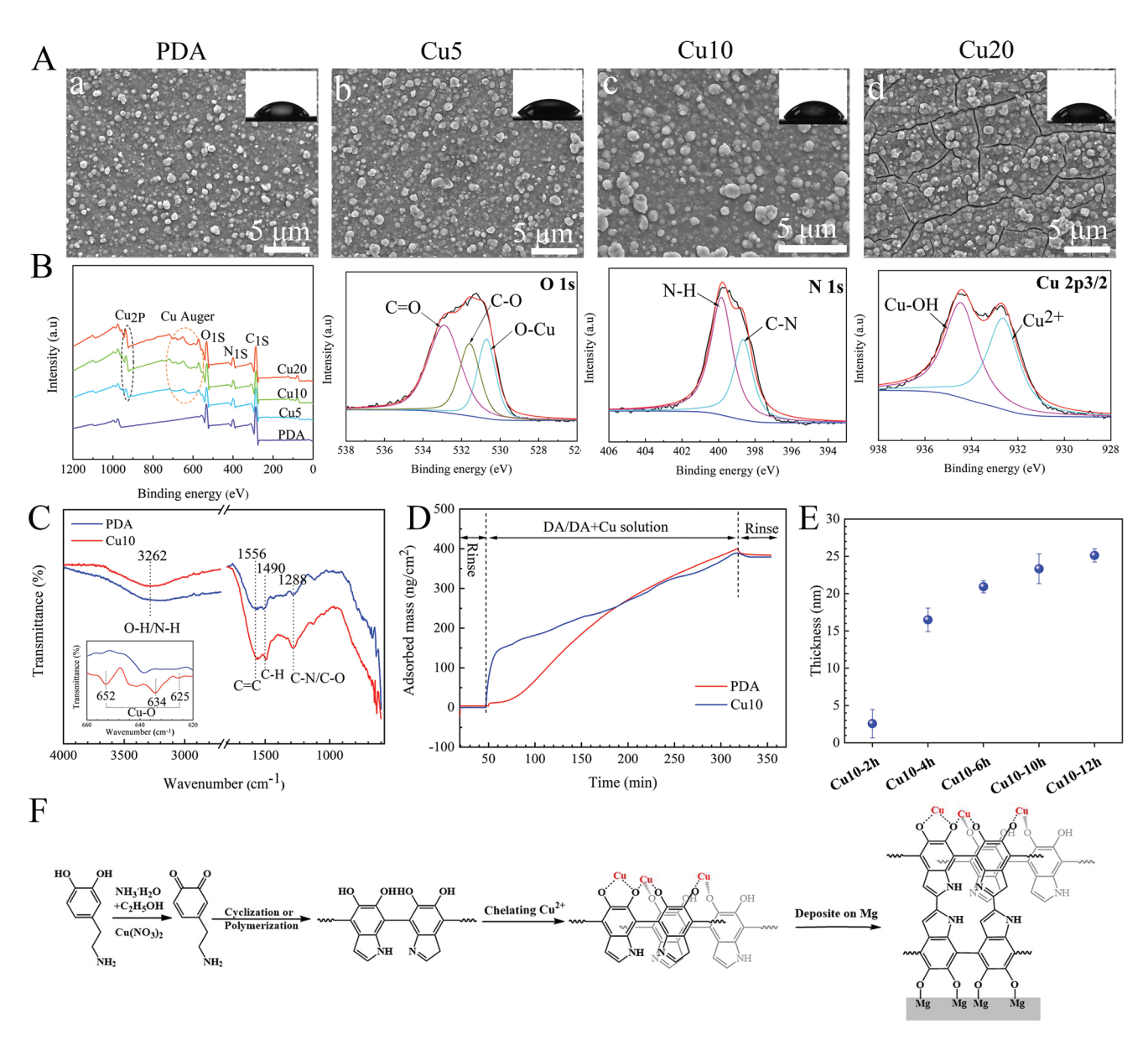


Figure 2. A) Surface morphologies and corresponding water contact angles of a) PDA, b) Cu5, c) Cu10, and d) Cu20 sample. B) XPS analysis of wide scans of PDA, Cu5, Cu10, and Cu20 samples and high-resolution spectra of O1s, N1s, Cu2p3/2 of Cu10. C) IR spectra of PDA and Cu10. D) Adsorption kinetics of PDA and Cu10. E) Thickness of PDA coating and Cu10 layer with different reaction time: 2, 4, 6, 10, and 12 h. F) Possible chemical reaction of copper-incorporated PDA coatings on Mg.

the Mg matrix through redox reaction, and in turn undermined the film quality.

The feasibility of the coating synthesis on Mg was further examined with X-ray photoelectron spectroscopy (XPS) and Fourier tansform infrared spectrometer (FT-IR) to clarify the composition and chemical structure of the obtained PDA and PDA/Cu(II) coatings. Figure 2B and Table S1 in the Supporting Information demonstrated the analysis of XPS survey spectra of all coated samples and high-resolution spectra of Cu10, confirming robust integration of copper (II) with varied content into PDA through this nonaqueous synthesis method. N 1s signal can be split into two peaks, N—H at 399.9 eV and C—N at 398.7 eV, typical of PDA. The apparent presence of Cu 2p peaks

and Cu Auger peaks verified the conjugation of copper, and the Cu $2p^{3/2}$ peak can be further divided into two, Cu-O (934.5 eV) and Cu²⁺ (932.7 eV). [22] Meanwhile, for O 1s, three intense signals were detected: aromatic C=O (532.9 eV), C-O (531.6 eV), and O-Cu (530.7 eV). These results indicated that the developing process of Cu incorporation is most possibly based on the chelation with the phenolic hydroxyl groups and quinone groups in PDA films. It is also noteworthy that although the surface content of Cu(II) exhibited a general increment trend from 1.33 to 2.58 at% with magnifying the feeding of Cu(NO₃)₂, it tended to reach a plateau with a O/Cu atomic ratio of \approx 6, presumably corresponding to the saturated coordination number in this system, a similar phenomenon as previously reported in



the iron and 3,4-dihydroxyphenylalanine (DOPA) chelation. [23] The characteristic FT-IR spectra of PDA and Cu10 measured with IR imaging microscopy were shown in Figure 2C, both of which revealed a similar broad peak at $\approx\!3262~\text{cm}^{-1}$ of O–H/N–H. The intense bands at 1556, 1490, and 1288 cm⁻¹ can be attributed to C=C, C–H, C–N/C–O of PDA and PDA-derivative. Additionally, new peaks of Cu–O at 652, 634, and 625 cm⁻¹ arose for Cu10 sample, [24] further confirming the above XPS evaluation of Cu(II) loading into PDA network through Cu–O bond.

To gain further insights into this Cu(NO₃)₂/ammonia-triggered reaction mechanism, quartz crystal microbalance with dissipation monitoring (QCM-D) was employed to monitor the in situ adsorption kinetics of polymer bound to the substrate surface (Figure 2D). The comparison between PDA and Cu10 clearly revealed that the addition of Cu10 acted as an effective trigger agent to sharply boost the deposition kinetics of the coating at initial stage. Correspondingly, Figure S1 in the Supporting Information displayed the solution color change with reaction time for comparison of DA and Cu10, and the corresponding macroscopic images of those on Mg substrates. The addition of Cu(NO₃)₂ significantly accelerated the polymerization process, as the corresponding reaction solution immediately turned into brownish black, a typical indicator of DA polymerization, whereas for single DA solution until around 2 h. The deposition kinetics is further quantified with PDA/ Cu(II) layer thickness on ultraflat model surface, ranging from 2.6 ± 1.9 to 25.1 ± 0.8 nm in prolonged reaction time (Figure 2E and Figure S2, Supporting Information), which generated

slightly increased surface nanoroughness (R_a) measured with Environment control scanning probe microscope (AFM; Figure S3. Supporting Information). Furthermore, we calculated the Cu(II) incorporation amount into PDA coating on Mg (Table S2, Supporting Information), with a surface density of $491.6 \pm 1.7 \text{ ng cm}^{-2}$ determined on the Cu10. In addition, the as-prepared PDA/Cu(II) layer exhibited excellent interfacial binding strength with the Mg substrate of 5B grade by standard test method for measuring adhesion tape test (ASTM D3359-09) (Figure S4, Supporting Information). As further demonstrated in Figure S5 in the Supporting Information, the PDA coating bound with the Mg substrate with strong chemical bonding of Mg-O (532.1 eV) through the catechol group presented in the PDA. Based on all these analyses, the possible synthesis mechanism of Cu-incorporated PDA coating on Mg using our nonaqueous synthesis method was proposed, as illustrated in Figure 2F.

2.2. In Vitro Mg Degradation Control and Ion Release

In vitro Mg degradation and the anticorrosion features of the as-prepared coatings were characterized by electrochemical corrosion and long-term immersion test, respectively, data of which were exhibited in **Figure 3**. According to Figure 3A, the steady open circuit potential (OCP) values of Cu5 and Cu10 were measured of -0.458 and -0.399 V, respectively, remarkably higher (more positive) than that of PDA (-1.354 V) and MgF₂ (-1.608 V). From the view of thermodynamics, it indicated a

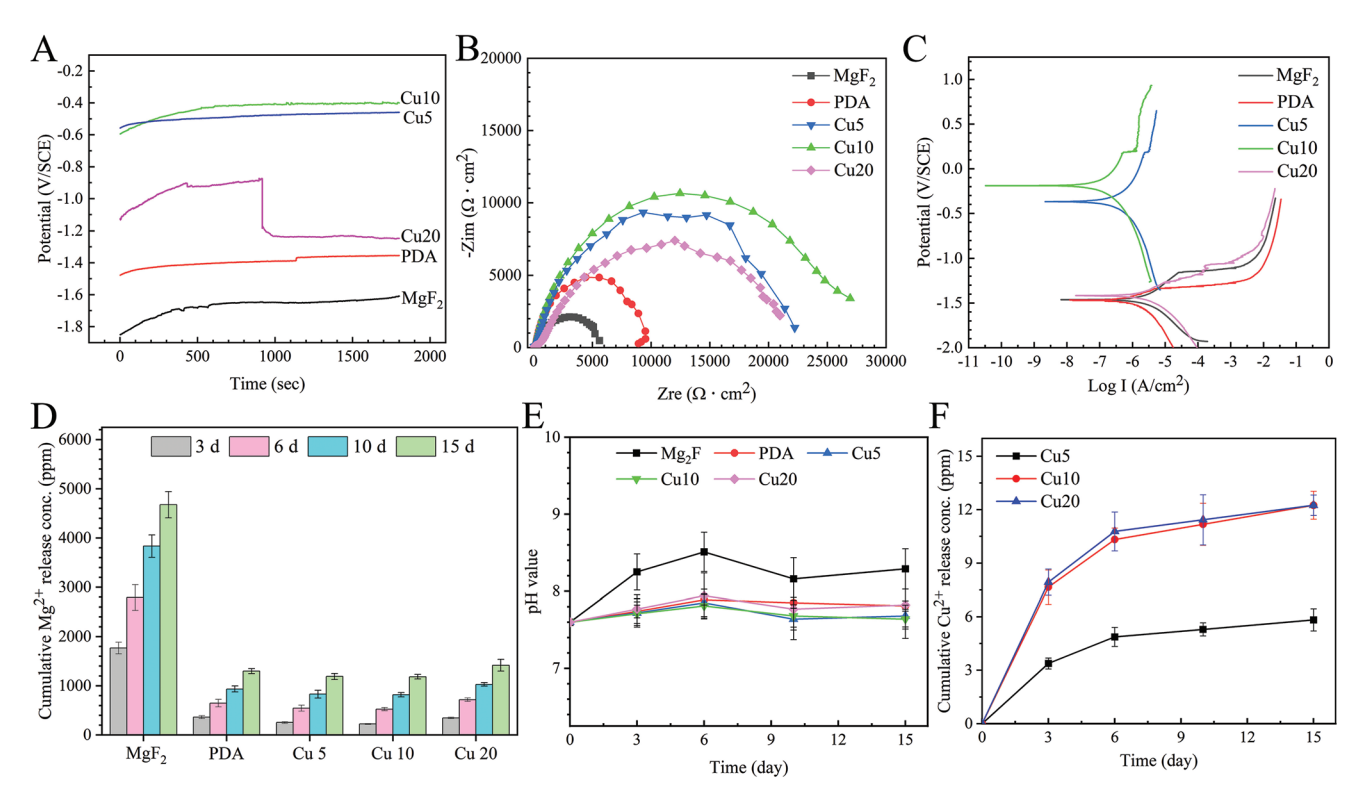


Figure 3. Electrochemical corrosion and long-term immersion measurements of MgF₂, PDA, Cu5, Cu10, and Cu20 samples. A) OCP plot, B) Nyquist plots, C) PDP curves, D) cumulative released Mg²⁺ concentrations, E) pH value, and F) cumulative release profile of Cu²⁺ upon immersion in cell culture condition.





 Table 1. Electrochemical corrosion parameters obtained from the polari

 Testion curves

Samples	E _{corr} [V _{SCE}]	i _{corr} [A cm ⁻²]
MgF ₂	-1.46	2.91×10^{-6}
PDA	-1.47	7.39×10^{-7}
Cu5	-0.34	2.72×10^{-7}
Cu10	-0.14	0.98×10^{-7}
Cu20	-1.42	3.63×10^{-6}

significant reduced Mg-corrosion tendency by the Cu5 and Cu10 treatment. Notably, a sharp decline of OCP occurs for Cu20 as its initial OCP value of −0.873 V drops to ≈-1.246 V, suggesting a breakdown of the original surface coating.^[25] The potentiodynamic polarization (PDP) curves were presented in Figure 3C, with fitted data of corrosion current density (i_{corr}) and corrosion potential (E_{corr}) summarized in Table 1. Consistently, Cu5 and Cu10 displayed preferable, potent corrosion-resistance among all the test samples, with $E_{\rm corr}$ of -0.336 and -0.142 V, and $i_{\rm corr}$ of 2.72×10^{-7} and 1.00×10^{-7} A cm⁻², respectively. However, insignificant enhancement in corrosion-resistance was observed for Cu20. It is thus apparent that the Cu10 group showed the best performance in enhancing corrosion-resistance of Mg, which considerably impeded the electrochemical corrosion kinetics by more than one order of magnitude as compared with MgF₂. The Nyquist plot of electrochemical impedance spectra (EIS) measurement was displayed in Figure 3B. The capacitive loop radius is usually utilized to evaluate the anticorrosion property of the coatings, in which larger capacitive loop radius indicates better corrosion resistance. The Cu(II)-coated groups displayed a much greater capacitive loop than the single PDA coating and MgF2. Additionally, Cu10 exhibited the largest radius of capacitive loop whereas Cu20 appeared the lowest, which was generally in agreement with the PDP analysis. To summarize the findings, the electrochemical corrosion resistance was initially enhanced with the increase of Cu content from Cu5 to Cu10, but drastically attenuated upon excessive supplement of Cu20, which severely disrupts the compactness of the coating structure.

In addition to the instantaneous electrochemical test, longterm immersion was also conducted under cell culture condition for further evaluation of actual in vitro degradation behaviors, reflected by the Mg²⁺ release and pH value profile (Figure 3D,E and Table S3, Supporting Information). It was worth noted that PDA and PDA/Cu(II) coating both remarkably decreased short-term and chronic degradation rate compared to the MgF₂ conversion layer. Explicitly, the initial released Mg²⁺ concentrations were obtained in the following order as: MgF₂ (1766.2 ppm) >> PDA (362.1 ppm) > Cu20 (346.3 ppm) > Cu5 (251.8 ppm) > Cu10 (222.2 ppm), namely, a further reduction by ≈87% in Mg degradation with Cu10 coating in comparison to the MgF₂ layer and an additional decrease by 40% against the single PDA film. By the end of the immersion test, the accumulated release amount of Mg²⁺ in the Cu10 group remained the lowest (1416.3 ppm), corresponding to a diminishment of ≈70% as compared with that of MgF₂ (4674.9 ppm). The pH evolution during immersion (Figure 3E) also followed a similar trend, in which the Cu-integrated groups constantly maintained close to the physiological pH of \approx 7.4, suggesting effective suppression of undue pH elevation of the MgF₂ group. In addition, SEM imaging indicated the Cu10 surface still kept intact without obvious sign of corrosion, in contrast to the MgF₂ group with a number of corrosion cracks after 15 d immersion (Figure S6, Supporting Information). It therefore further indicated the efficient long-term corrosion control of PDA/Cu(II) coating for of Mg-based biomaterials.

The eluted Cu²⁺ from PDA/Cu(II) complex network during the in vitro Mg degradation process was also measured (Figure 3F), which revealed a controlled, sustained release profile in at least 15 d for all three groups. Specifically, a more rapid release characteristic of Cu2+ within the first 3 d could be observed, which then gradually slowed down. As compared to the Cu5 group, the Cu10 and Cu20 displayed remarkably higher release rates and cumulative release amounts of Cu²⁺, corresponding to the elevated loading concentrations in the asprepared polymer coatings. The cumulative eluted Cu²⁺ from Cu10 and C20 by the end of the 15-d test thus reached a moderate concentration of 12.2 \pm 0.7 ppm (with the standard sample surface/solution volume ratio of 1.25 cm² mL⁻¹), which doubled that of Cu5 (5.8 \pm 0.6 ppm). Notably, the Cu10 and Cu20 exhibited nearly identical Cu(II) release kinetics profiles, which is in agreement with the aforementioned XPS results of similar Cu atomic ratios in the as-prepared coatings.

Mg and its alloys degrade spontaneously in the aqueous environment via an electrochemical corrosion, producing magnesium hydroxide and hydrogen gas. After a general hydrofluoric acid (HF)-treatment, MgF2 conversion layer with thickness of micrometers would be formed. Nevertheless, this layer could only reduce the degradation rate of Mg alloys in the initial stage while lacking chronic effectiveness and satisfactory biocompatibility. [26] Many other coating techniques, including previously reported PDA coating method, often suffered from some major drawbacks, such as poor adhesion, peeling-off, porous, or defective microstructure. To provide adequate protection for biodegradable Mg matrix in long-term services still remains a critical concern.[21] In this work, combining the results of electrochemical and long-term immersion tests, it was apparent that Cu10 increased the corrosion-resistance of Mg substrates to the greatest extent among all the test groups. As illustrated in Figure S7 in the Supporting Information, the anticorrosion mechanism of Cu10 was then proposed of twofold: 1) oxidation of PDA-based coating with Cu(II) during polymerization reaction impede the thermodynamic tendency of corrosion and 2) chelation of Cu(II) into the PDA network led to a more compact, reinforced microstructure of the passive film to retard corrosion kinetics. Actually, this copper-integrated PDA coating not only further improved chronic corrosion-resistance for Mg but also provided versatile biofunctions, displayed as follows.

2.3. Hemocompatibility

It was reported that rapid degradation of Mg would induce an excessive increment in local pH of the blood and trigger the combination of red blood cells and Ca²⁺ ions in the solution, leading to the rupture of red blood cells and serious hemolytic reaction.^[27] The hemolysis rates of naked JDBM, MgF₂,





www.afm-journal.de

and Cu10-coated samples were therefore carefully examined, as exhibited in Figure S8 in the Supporting Information. According to the International Organization for Standardization (ISO) 10993-4:2020 criteria for clinical application, the hemolysis rates of naked JDBM (5.88%) and MgF₂ (5.4%) both slightly exceeded the standard of 2%, though greatly lower compared to many other Mg alloys with hemolysis rate over 50%. [28,29] With Cu10 surface treatment on JDBM matrix, it even achieved a complete elimination of hemolysis rate (0.044%) and thus well fulfilled the clinical requirement, owing to the more effective degradation control of Mg. The resultant PDA/Cu(II)-Mg system was thereby endowed with superior potential in preventing hemolysis and subsequent fatal risk.

In addition, at the early stage of postimplantation, thrombogenesis involves a series of biochemical processes such as platelet aggregation, coagulation, and fibrinolysis. [30] Therefore, in vitro platelet adhesion was also evaluated on the coated Mg, with the use of Co—Cr and naked Mg as the controls (Figure S9, Supporting Information). It can be clearly seen that a large number of platelets were attached onto the Co—Cr surface, though most of inactivated state with their pseudopodia fairly extended. In contrast, adherent platelet number was enormously reduced on all the Mg-based specimens, with the Cu10 revealed the lowest (p < 0.0001 vs Co—Cr). Besides, almost all the platelets retained their original round morphology and presented no evidence of activation. The results thus indicated the PDA/Cu(II)-Mg system remarkably inhibited the risk of platelet adhesion.

2.4. Direct Cell Assay on Coated Mg

Rapid endothelialization on the cardiovascular stents postsurgery is essential for mitigating the occurrence of in-stents thrombosis and restenosis.^[31] In addition, the development of atherosclerosis and neointimal lesion formation in blood vessel directly correlates to the excessive VSMCs adhesion and proliferation.[32] Therefore, we then investigated the responses of VECs and VSMCs to MgF₂, PDA, and PDA/Cu(II) coated-Mg, respectively, particularly in regard of direct cell adhesion and proliferation (Figure 4). In accordance with its poor anticorrosion performance (Figure 3), MgF2 group revealed a general inhibition on both VECs and VSMCs activity with largely reduced adherent cell density. Notably, there appeared a large portion of dead VECs attached (Figure 4A), presumably attributed to the disrupted microenvironment under excessive Mg corrosion with MgF₂-coated Mg. On the contrary, in the PDA group both cells exhibited excellent viability with a significant boost as compared with the blank control (Figure 4A,C), suggesting a better interfacial condition provided by PDA to support cell adhesion and proliferation. Nonetheless, this stimulatory impact with PDA coating was much more prominent on VSMCs (Figure 4B,D), showing the highest activity among all the specimens, which is often considered undesirable in view of potential neointimal hyperplasia.

Most impressively, the PDA/Cu(II) coatings on Mg exhibited a striking augment on VECs adhesion, spreading, and proliferation compared to both the blank control and the PDA group (p < 0.001), following an order of Cu10 > Cu5 > Cu20. It is

noteworthy that after 3 d-culture the VECs density in Cu10 group reached a dramatic increment of 3.7-fold versus blank control, and 2.4-fold of the PDA group. Meanwhile, for Cu5 and Cu10 groups, the VSMCs adhesion and growth were substantially suppressed in comparison to the PDA (p < 0.001) and the blank (p < 0.01), while insignificant inhibitory effect was found for the Cu20. Apparently, the ratios of VECs to VSMCs were remarkably enhanced by the Cu(II)-incorporated coatings on Mg, as shown in Figure 4E. Furthermore, Cu10 provided the most compelling selectivity for VECs over VSMCs (p < 0.001), which was quantified as 5.1 times greater than the control group after 3 d-culture. These results suggested that apart from the prominent influence of Mg degradation, an appropriate Cu incorporation in the PDA coating, is equally vital to modify cellular microenvironment and in turn to direct interfacial behaviors of vascular cells. Collectively, Cu10 provides exceptional merits in both Mg degradation control and beneficial vascular cell selectivity of promoting VECs activity while restraining VSMCs. Therefore, in the following investigations we concentrated on the samples with Cu10 surface treatment.

Nitric oxide (NO), mainly produced by endothelial nitric oxide synthase (eNOS) on the membrane of VECs, is well recognized to maintain vascular homeostasis, including regulating local cell growth, normal endothelial function, and proper blood flow and pressure. As the NO secretion evaluation in Figure 4F demonstrated, while insignificant distinction of NO generation among MgF₂, PDA and the control groups, Cu10 significantly evoked enhanced activity of NO release of VECs (p < 0.01). In fact, bioinspired NO-based therapy has recently been formulated for the treatment of CAD to alleviate ISR and thrombosis postimplantation,^[33] the majority of which required employment of NO donors (e.g., S-nitrosothiols) or biocatalysts into the stent coatings to enable the chemical storage and subsequent delivery of NO in either systemic or local manner. Distinct from this exogenous NO release strategy, this proposed Cu(II)-incorporated Mg system offered an effective platform to promote endogenous NO release from VECs, with aforementioned differential modulation of VECs and VSMCs growth achieved. We then hypothesized the Cu²⁺ ions eluted from the coating and the released Mg²⁺ with degradation of Mg alloys may hold collective responsibility for the resultant bioactivity in the absence of NO donors or biocatalysts. Further investigation to elucidate the underlying molecular biological mechanism was thus explored in the following.

2.5. Effect of Released Metallic Ions on Vascular Cell Behaviors and Underlying Mechanism

We then studied the corresponding impact of the metallic ions eluted from the Cu10-coated JDBM on the response of VECs and VSMCs. Specifically, the extracts containing both released Cu²⁺ and Mg²⁺, single Cu²⁺, and single Mg²⁺ were prepared and subjected to study. For VECs (**Figure 5A**), compared to the blank group, the combination of Cu²⁺ and Mg²⁺ significantly promoted VECs viability, whose effect was even more remarkable after 3 and 5 d culture (p < 0.001). On the contrary, single Mg²⁺ revealed slight inhibitory effect on VECs and single Cu²⁺ appeared similar as the blank. In the case of VSMCs

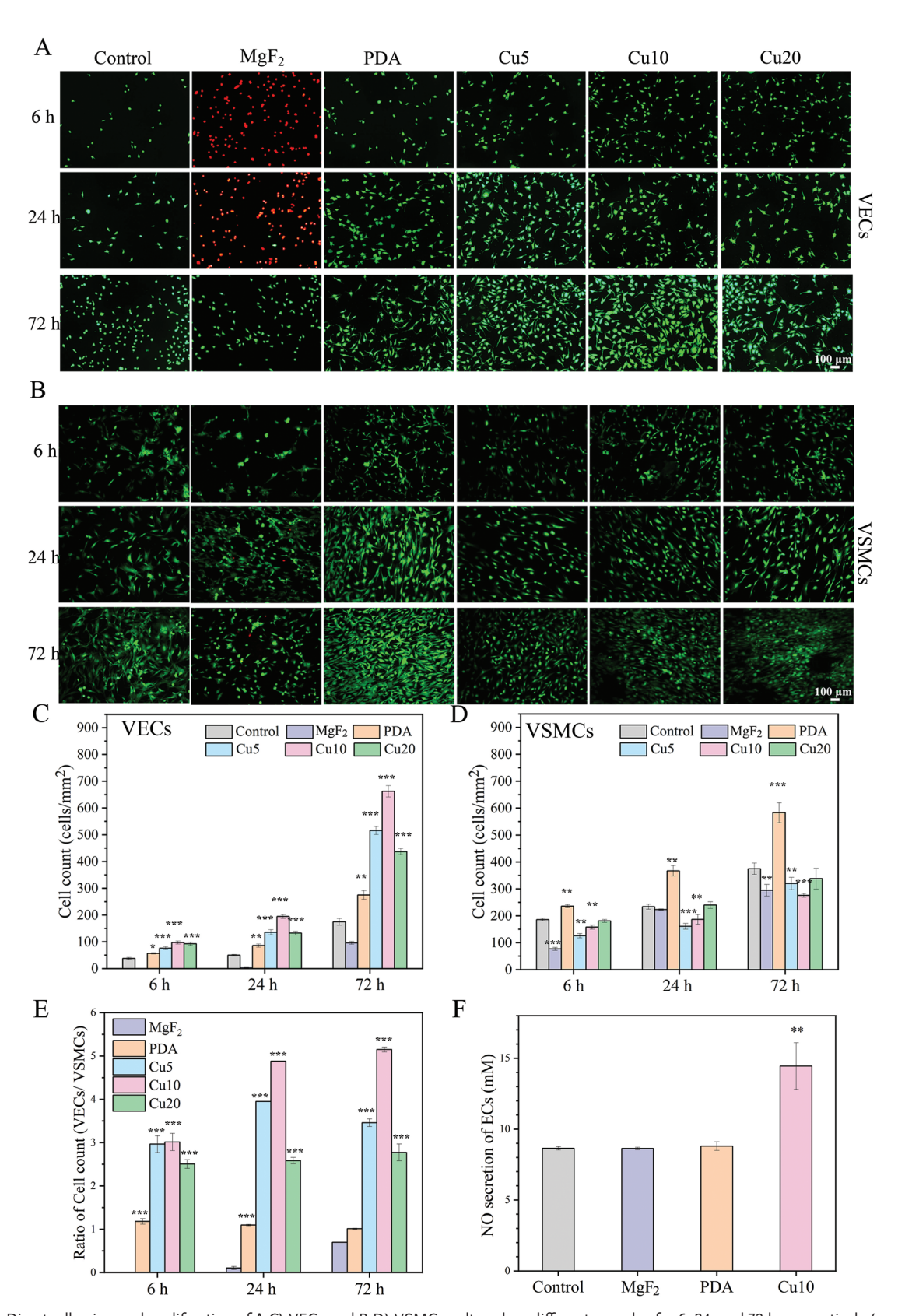


Figure 4. Direct adhesion and proliferation of A,C) VECs and B,D) VSMCs cultured on different samples for 6, 24, and 72 h, respectively (n = 6). E) Calculated ratios of VECs to VSMCs, normalized by the ration of the blank control group. F) NO secretion of VECs. Statistically significant differences are compared with the control group (n = 6). (Data presented as mean \pm SD and analyzed using a one-way ANOVA with Tukey post hoc test, *p < 0.05, **p < 0.01, ***p < 0.001).

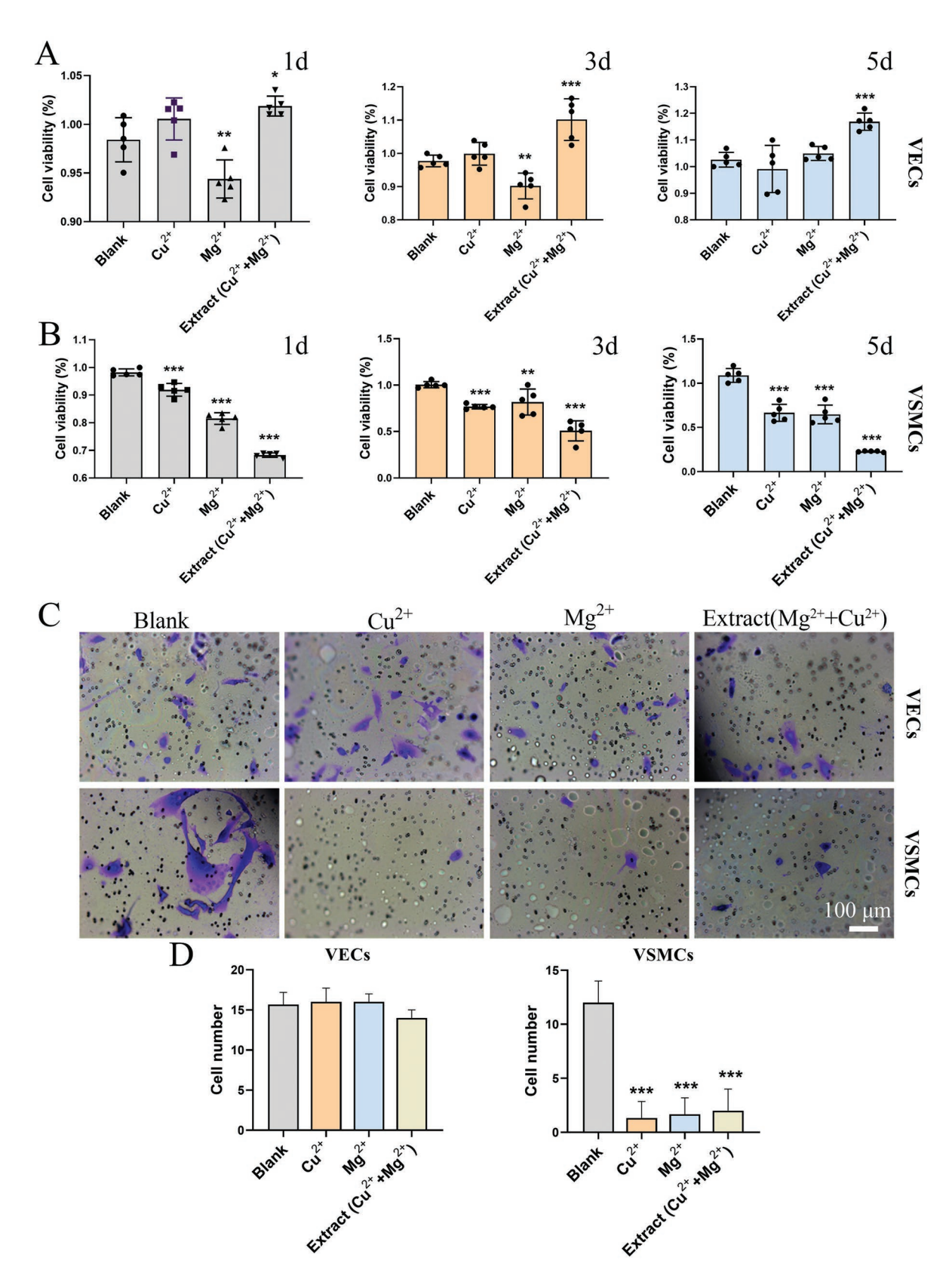


Figure 5. Cell viabilities of A) VECs and B) VSMCs for 1, 3, and 5 d, respectively (mean \pm SD, n = 5 independent samples). C) Representative microscopic images of VECs and VSMCs migration assay and D) corresponding evaluation of cells migration (mean \pm SD, n = 5 independent samples). One-way ANOVA with Tukey post hoc test, *p < 0.05, **p < 0.01, ***p < 0.001.





www.afm-iournal.de

(Figure 5B), all the three groups suppressed VSMCs viability and growth, among which that containing both Cu²⁺ and Mg²⁺ displayed the most intense inhibitory effect on VSMCs compared to single Cu²⁺ or single Mg²⁺. Possible influence on cell migration was also examined (Figure 5C,D). Insignificant difference was found among all the groups, that is, neither the eluted single Cu2+, single Mg2+ nor the counterpart of their combination exerted any adverse effect on VECs migration. Additionally, no detriment was caused to the tube formation of VECs (Figure S10, Supporting Information). Meanwhile, all three groups considerably undermined VSMCs migration, implying promising potential for suppressing in vivo neointimal formation. Based on these evaluations, it is most probably the synergetic function of moderate released Mg²⁺ and Cu²⁺ that served as a biochemical cue to foster VECs viability and bioactivity, and simultaneously to impair the proliferation and migration of VSMCs.

To disclose the molecular mechanism of which the Cu(II)incorporated Mg system simultaneously promote VECs and inhibit VSMCs, we performed RNA sequencing (RNA-seq) after cells had been cocultured with them. A volcano plots illustrate the large number of transcript abundance differences on its influences of VSMCs. 427 genes were identified as downregulated (Log₂fold change (FC) < -1; p < 0.05) and 423 genes were upregulated (Log₂(FC) > 1; p < 0.05; Figure 6A). Then, gene ontology (GO) function enrichment and Kyoto Encyclopedia of Genes and Genomes (KEGG) pathway analysis confirmed these differentially expressed genes (DEGs) were mainly related to inflammatory associated pathways, which were enriched in tumor necrosis factor alpha (TNF- α) signaling pathway (Figure 6B). Besides, the heat map of DEGs (Figure 6C) presented significant upregulation of interleukin-1 β (IL1 β) and NLRP3, which were potent proinflammatory cytokines^[34,35] and this was further validated by the western blotting analysis (Figure 6D). It is well known that NLRP3 is the key member of the inflammasome, which is responsible for the release of damage mediators during cell or tissue injury to activate an inflammatory response.[36] In our case, NLRP3 inflammasome was triggered by the Mg-Cu(II) system and further cleaved IL1 β , a powerful proinflammatory cytokine and demonstrated to inhibit VSMCs activity by inflammatory reaction, into active proinflammatory mediators by activating caspase-1.[37] Therefore, a killing role on VSMCs through inflammatory reaction was proposed in this system.

With respect to VECs, 871 downregulated and 993 upregulated DEGs were resolved (Figure 6E). Enrichment analysis for processes run on the DEGs from each comparison revealed significant enhancement for angiogenesis signaling (Figure 6F). We found the Mg-Cu(II) system induced elevated expressions of several of the most important angiogenic factors, including fibroblast growth factor 1 (FGF1), epidermal growth factor (EGF), and angiogenin-4 (ANGPT4) (Figure 6G). In addition, the upregulation of EGF expression was further supported by the enzyme linked immunosorbent assay (ELISA) quantification (Figure 6H). The activation of EGF plays a fundamental role in facilitating the endothelial cell's survival, proliferation, migration, and further protecting angiogenesis. Section 1967, an important member of FGF family, has also been reported to boost the proliferation, migration and survival of VECs in

many tissues.^[41] Moreover, ANGPT4 is known to be involved in enhancing vein specific development and playing a pivotal role in venous remodeling, retinal fluid clearance, and neuronal function.^[42]

Taken together, we revealed a previous unknown, biphasic role of Cu(II)-incorporated Mg system on differential directing the fate of VECs and VSMCs, ascribed to the synergistic effect of Mg²⁺ and Cu²⁺, as illustrated in Figure 6I. Endothelialization could be encouraged through a series of signaling pathways associated with VECs viability and endothelial functions, involving EGF, FGF1, and ANGPT4. Meanwhile, the activation of NLRP3/IL1 β signaling pathway contributed to the inhibitory effect on VSMCs, which is believed to be beneficial to mitigating neointima hyperplasia and restenosis.^[36]

2.6. In Vivo Stent Implantation

Stent implantation was then performed to demonstrate the biosafety and efficient performance of the PDA/Cu(II) as multifunctional engineering of a vascular device coating. In this study, the MgF2-coated and Cu10-coated JDBM vascular stents were respectively implanted into abdominal aorta of New Zealand white rabbits, as shown in Figure 7A-C. Cu10 coating was uniformly distributed on the JDBM stent, which displayed no cracked or peeled condition upon stent dilation (Figure 7B). All the stent groups did not exhibit noticeable systemic or local toxicity. In vivo re-endothelialization in the early stage was carefully examined for the two Mg-based stent groups in comparison with the Co-Cr control group. After 7 d implantation (Figure 7D), CD31 staining suggested that only the Cu10 stents surface was well adherent with an intact layer of VECs, suggesting rapid re-endothelialization could be accomplished with 1 week. On the contrary, little was found on the struts of MgF₂ and Co-Cr groups. At 14 d (Figure 7E), the Cu10 coated JDBM stent surface was completely covered by compact endothelial multilayer. For comparison, the Co-Cr stent just completed reendothelialization with a very thin layer of VECs attached and MgF₂ stent was only partly covered by VECs (≈80% coverage), which were further confirmed with SEM imaging (Figure 7F). In addition, there appeared no obvious platelet, fibrin, or inflammatory cells on Co-Cr, MgF₂, or Cu10 stents.

Meanwhile, the surface elements of the Cu10 stent before and after 14 d implantation were detected by SEM-EDS (energy dispersive X-ray spectroscopy) to obtain the information on the in vivo Cu²⁺ release (Figures S11 and S12 and Tables S4 and S5, Supporting Information). At 14 d, as compared to the original coating surface, the copper content was decreased from 0.44 \pm 0.050 to 0.25 \pm 0.051 at%, which demonstrated a sustainable release maintained for at least 2 weeks in vivo, with approximately half of the initially loaded Cu(II) on the stent eluted. This result corresponds to a calculated release amount of $\approx\!279.3\pm1.6$ ng cm $^{-2}$ of copper within the first 2 weeks postimplantation. It hence indicated the Cu(II)-coated Mg stent system enabled a controlled, moderate release of Cu $^{2+}$ ions which in turn played a vital role in the promoted early re-endothelialization.

Next, 1 and 3-month follow-up was carried out to investigate the bioeffects and degradation of the coated-Mg

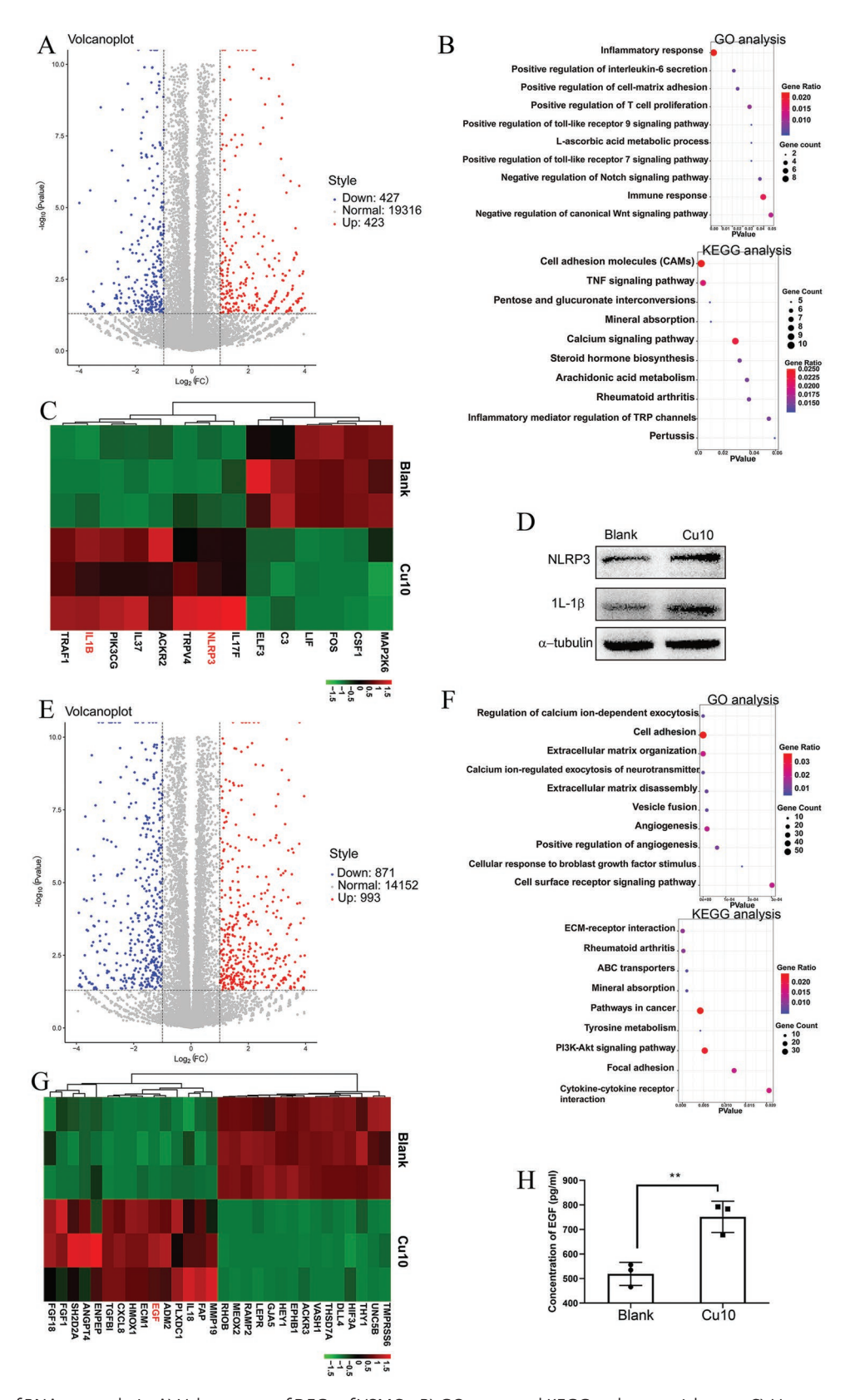


Figure 6. Results of RNA-seq analysis. A) Volcano map of DEGs of VSMCs. B) GO terms and KEGG pathway enrichment. C) Heatmap of DEGs of VSMCs in blank and Mg-PDA/Cu(II). D) Western blot analysis of blank and Mg-PDA/Cu(II). E) Volcano map of DEGs of VECs. F) GO terms and KEGG pathway enrichment. G) Heatmap of DEGs of VECs in blank and Mg-PDA/Cu(II). H) Concentration of EGF by ELISA assay (mean \pm SD, n = 3 independent samples, by two-tailed unpaired Student's t-test, **p < 0.01). I) Illustration of the EGF signaling in VECs and NLRP3 and IL1 β signaling in VSMCs.

www.afm-journal.de

d by only 7.92% and 17.6%,
elmingly reduced by \$20.1%

stents. A number of platelets with irregular discoid shape in 5-7 µm diameter appeared on MgF₂ after 1-month implantation. At 3 months, MgF2 stents surface was often evidenced with obvious corrosion cracks and corrosion products, with incomplete or impaired endothelialization. In contrast, SEM (Figure 8A) further confirmed intact endothelium maintained full coverage for the entire surface of Cu10 stents. According to optical coherence tomography (OCT, Figure 8B), digital subtraction angiography (DSA) and intravascular ultrasound (IVUS, Figure S13B,C, Supporting Information) characterization, no apparent in-stent thrombosis, restenosis, or severe neointimal hyperplasia was found in both of the two coated-Mg stents during the entire period. The Cu10 group consistently showed distinct stent strut profile, whereas the MgF2 group exhibited a marked weakening, blurred signal, attributable to the inefficient corrosion protection for Mg matrix with MgF₂ coating over long term. In addition, Hematoxylin-eosin (HE) staining (Figure 8C) revealed greatly reduced neointimal formation on the lumen of Cu10-coated JDBM stent after implantation for 1 and 3 months, in comparison with the MgF₂. Quantitative analyses of injury score, inflammation score, and intimal area were presented in Figure 8D. Vessel injury was markedly diminished in Cu10 group (injury score 1) after 3 months when compared to the MgF₂ group (score 3), most possibly due to better control of Mg stent degradation with Cu10. As for inflammation, the MgF₂ group also exhibited a relatively high score (score 3), while a significant amelioration of inflammation level was achieved with Cu10 coating, particularly in the first month postsurgery. To access the performance on neointimal hyperplasia and restenosis, it suggested the neointimal area of Cu10-coated JDBM stent significantly decreased by ~50% in comparison to the MgF2 stent after 1 month implantation, which remained constantly low for Cu10 group at 3 months.

In vivo degradation behaviors of both Mg-based stents were quantitatively assessed by X-ray microscope (XRM) analysis as it determines the durability for effective scaffolding capacity. As shown in Figure 8C and Figure S14 in the Supporting Information, after 1 and 3 months' implantation, the total volume

of Cu10 stent gradually decreased by only 7.92% and 17.6%, whereas MgF $_2$ stents was overwhelmingly reduced by $\approx 20.1\%$ and 36.6%, respectively. Most impressively, Cu10 stent still kept its main structure integrity in the end of 3-month implantation, while MgF $_2$ stent completely lost its original shape, left with a number of corroded pieces. The acquired in vivo degradation data thus confirmed a potent anticorrosion effect with PDA/Cu(II) coating to modulate appropriate Mg-based stent degradation profile and ensure long-term scaffolding durability.

In this work, the integration of biological functional of magnesium ions and construction of polymer coating network is currently a huge challenge. Thus, the traditional DES techniques may not be suitable for Mg alloy, as it inevitably increases late incidence of adverse events. The Mg-PDA/Cu(II) system not only effectively improved the degradation regulation of the stents but also utilized the synergetic effect of controlled released Mg²⁺ and Cu²⁺ ions, which were both modulated with the Cu(II)-integrated coating. Moreover, it was observed to be capable of initiating rapid endothelialization in 7 d, among the most favorable results achieved on vascular stents in rabbit model to date.[30] Accordingly, we introduce this type of multifunctional surface modification approach particularly for biodegradable metals as an "AIM" (namely, active interplay with the matrix) coating strategy. The designed coating not only amends the rapid corrosion drawbacks of the matrix but also tailored active interaction with the matrix Mg to exert mutual biochemical effect, consequently bringing out remarkably enhanced in vivo outcomes. In-depth understanding of the mechanisms beneath the AIM methods would in turn facilitate harnessing the therapeutic power of the matrix materials and their degradation products. We therefore anticipate the employment of this "AIM" idea in designing functional coating for biodegradable matrix could pave a nascent, niche avenue for advancing the development of bioresorbable metal-based biomaterials and devices in a broad variety of regenerative medicine applications, while in vivo bioefficacy needs to be further investigated in diseased model and in the longer term even after the full degradation of the implants for potential clinical use.

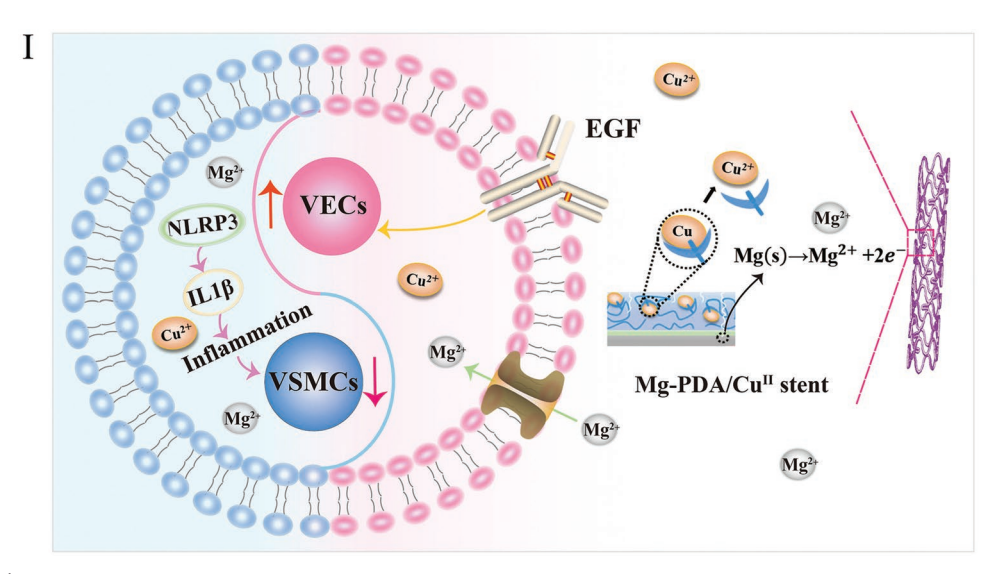


Figure 6. Continued

www.afm-journal.de

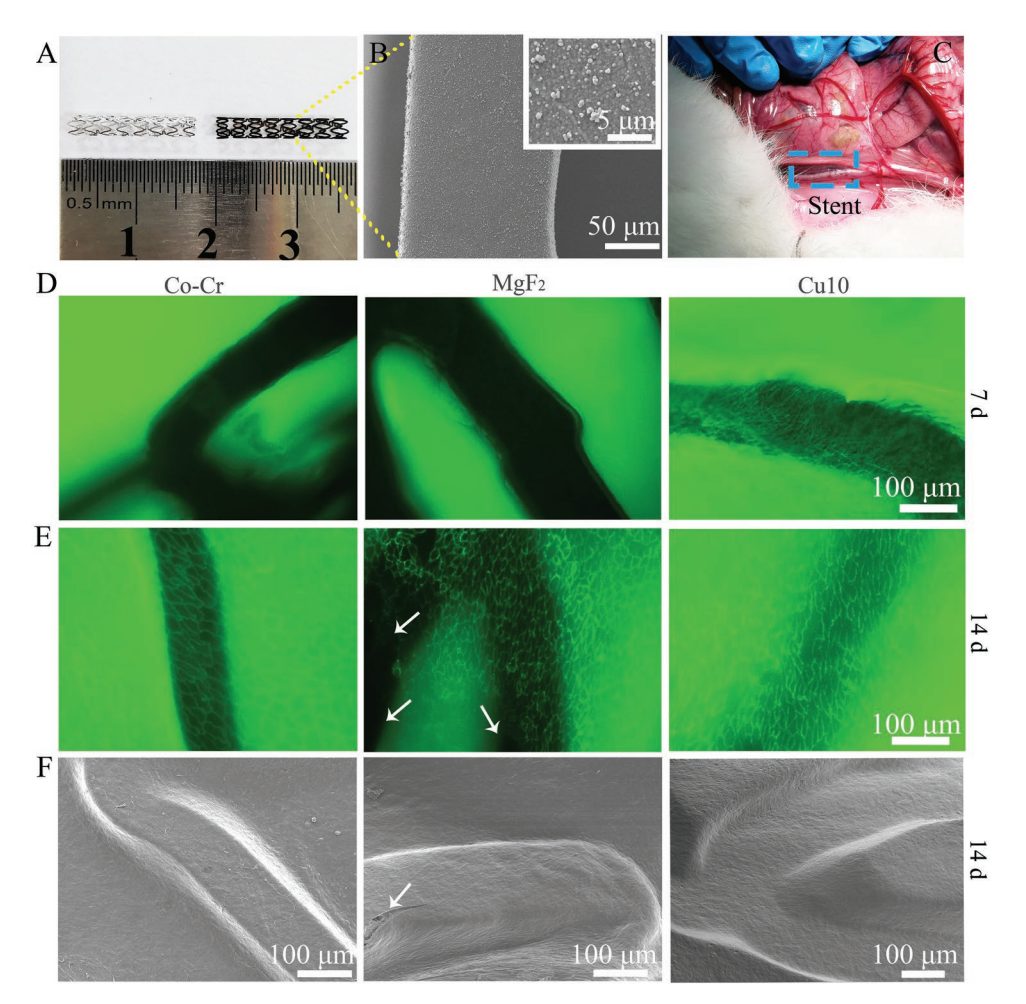


Figure 7. A) Photographs of JDBM and Cu10 stent. B) SEM images of Cu10 stent. C) Representative images of Cu10 stent implanted into the abdominal aorta under angiographic control. D,E) CD31 fluorescence image after 7 and 14 d implantation. F) Corresponding SEM results of the harvested stent after 14 d implantation.

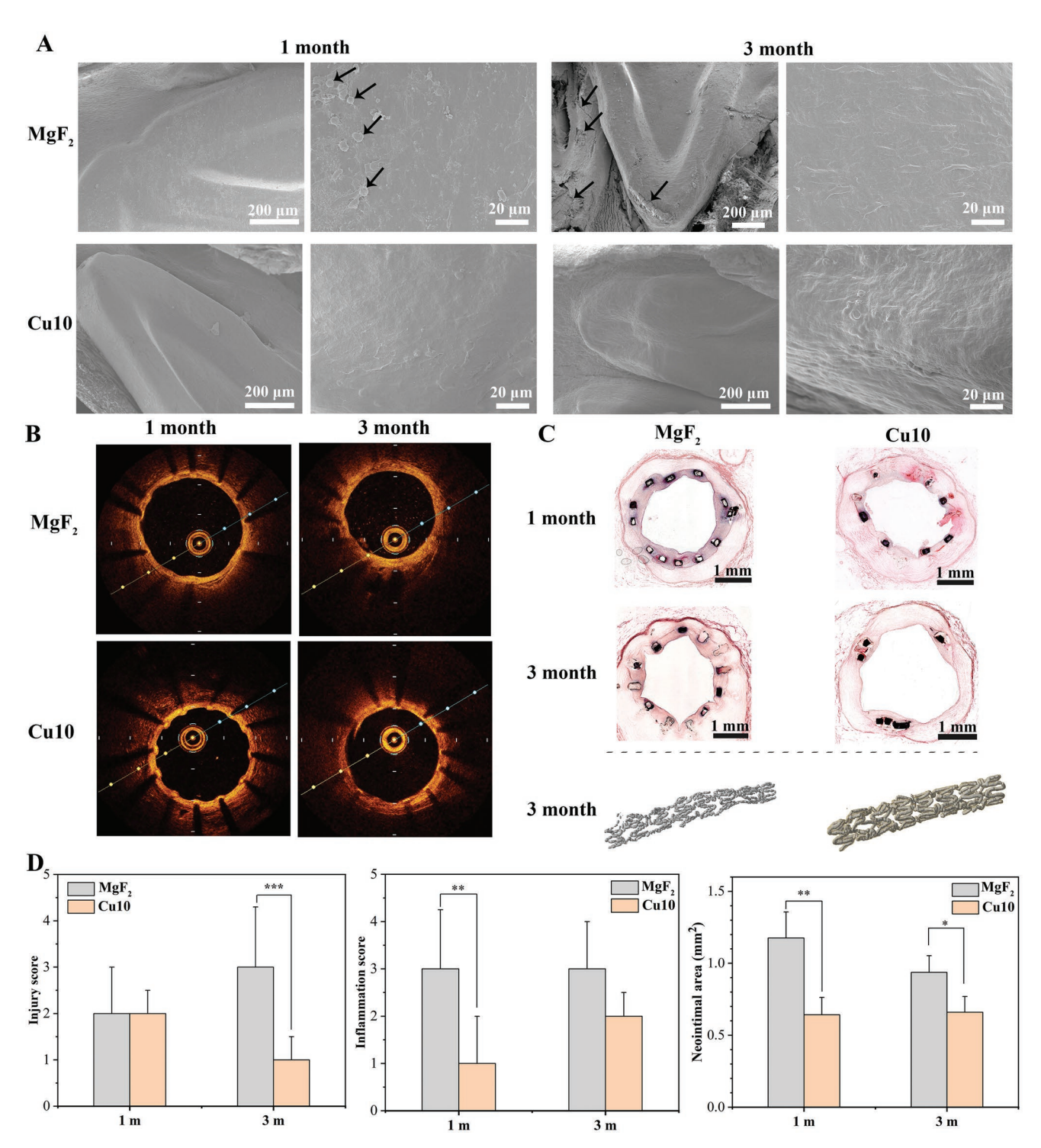
3. Conclusion

In summary, we introduced a thin, compact film of Cu(II)incorporated polydopamine for biodegradable Mg alloy stents with reinforced corrosion-resistance and favorable biofunctions. The optimized chelated copper endowed the stent system with significantly accelerated film deposition, formulated intact coating structure, retarded Mg degradation, and sustained release of Cu2+. In addition, the generated Cu(II)-integrated Mg remarkable promoted VECs growth and endogenetic NO release, while simultaneously inhibited VSMCs. Such desirable cell selectivity was attributed to the synergetic bioeffect of locally released Mg2+ and Cu2+ ions, associated with the upregulated expressions of EGF, FGF1, and ANGPT4 in VECs and activation of NLRP3/IL1 β inflammation signaling pathway in VSMCs. In vivo implantation study further confirmed the Cu(II)-Mg alloy stent could enhance scaffolding durability, facilitate rapid re-endothelialization, and alleviate neointimal hyperplasia, without obvious injure, inflammation, or thrombosis. The proposed multifunctional coating strategy on Mg as demonstrated in this proof-of-concept study is hence believed to inspire the development and deployment of next-generation biodegradable implants to exploit their full potential for compelling outcomes.

4. Experimental Section

Materials and Fabrication of Mg Vascular Stent: Disk samples used in vitro were cut with a dimension of $\Phi 14~mm \times 3~mm$. Sample surface was mechanically ground using silicon carbide papers progressively from 300 to 3000 grit, then ultrasonic in ethanol for 10 min, and finally dried with warm air. The detailed new shape optimization framework of Mg vascular stent was demonstrated in the previous work. After pulsed laser cutting, annealing, and electropolishing, JDBM stent was ultrasonic in ethanol for 10 min and finally dried with cool air.

Preparation of PDA/Cu(II) (Cu5, Cu10, and Cu20) Coating: All samples were pretreated in HF for 12 h. To fabricate PDA coating with nonaqueous phase polymerization, dopamine hydrochloride was first dissolved in ethanol with a conc. of 2 mg mL⁻¹ upon ultrasonication. Then, ammonia water was added, which generated a final 95 vol% of ethanol and 5 vol% of ammonia water content in the mixture of the DA solution. Pretreated MgF2-IDBM (or other substrate, e.g., silicon wafer) was immersed into the freshly prepared DA solution for 12 h and repeated for five times to reach a thickness of \approx 100 nm. For preparing the outermost layer of Cu(II)/PDA, a Cu(NO₃)₂ stock solution (0.5 M) was prepared by dissolving Cu(NO₃)₂ *3H2O in ethanol. Different



amount of the stock solution was added into the aforementioned DA ammonia/ethanol solution to reach a Cu(II) concentration of 5, 10, and 20 mm respectively. Samples were immediately immersed into this mixture solution with a reaction time of 12 h to obtain the deposited Cu(II)/PDA coating, which were correspondingly denoted as Cu5, Cu10, and Cu20. In each process, the treated samples were first rinsed with

deionized water, and subsequently ultrasonically cleaned in ethanol two times (each for 5 min) to remove unreacted substances and weakly bonded species, and finally blown dried with a stream of nitrogen gas.

Surface Characterization: The sample surface morphology was observed by SEM (Mira3, TESCAN, Czech). Chemical bond of coating was identified by XPS (AXIS Ultra DLD, Kratos, Japan) and Fourier





standard solution and collected supernatant was transferred into a new 96-well plate and then 50 μL of Griess Reagent I and Griess Reagent II were added respectively. OD value was measured at 490 nm by microplate reader (iMARK, Bio-Rad, USA) and normalized.

transform infrared spectrometer (FT-IR, Nicolet 6700, Thermo Fisher, USA). Water contact angles were evaluated using a contact angle goniometer (JC2000D1, China). Thickness of the coating was measured by Environment control scanning probe microscope (AFM, Nanonavi E-Sweep, Japan). QCM-D (Qsense-E4, Biolin Scientific, Sweden) was utilized to analysis the adsorption kinetics of PDA and Cu10 coated on Mg alloys. Testing was conducted at 25 °C and a flow rate of 20 µL min⁻¹. After establishment of a stable baseline using 4-(2-hydroxyethyl) piperazine-1-ethanesulfonic acid (HEPES) buffer solution, the polymer solution was allowed to flow through the system for 4 h 20 min. Subsequent rinsing by ultrapure water, bonding strength between PDA/Cu(II) coating and Mg substrate was measured by Tape test according to ASTM D3359-09 standard test methods.

In Vitro Degradation Evaluation: HF-treated (MgF2), PDA coating, Cu5, Cu10, and Cu20 samples were carried out electrochemical tests at 37 ± 0.1 °C in Hank's solution. A typical three electrode system (DH7000, DONGHUA, China) with platinum plate as counter electrode, saturated calomel electrode (SCE) as reference electrode, and Mg samples with exposed area of 1 cm² as working electrode was applied. OCP test was performed 1800 s. EIS measurements were performed over a frequency range from 100 kHz to 0.01 Hz versus OCP. PDP was conducted from -500 to 1300 mV_{SCF} versus OCP at a scan rate of 1 mV s⁻¹. Immersion test of Mg specimens were also measured in Dulbecco's modified Eagle medium (DMEM, Gibco, USA) medium in CO2 incubator at 37 °C with a surface/volume ratio of 1.25 cm² mL⁻¹ (according to ISO 10993-5) for different durations (3, 6, 10, 15, and 23 d), respectively in triplicate. At that end point, the concentrations of metallic ions in collected medium and the blank control medium were measured by inductively coupled plasma optical (ICP, iCAP6300, Thermo, USA). The obtained ion release conc. was subtracted with that in the blank control.

Cell Adhesion and Proliferation Tests: Vascular endothelial cells (VECs) and vascular smooth muscle cells (VSMCs) (8000, Sciencell, USA) were seeded on the sample surface with a density of 2×10^4 cells mL⁻¹ in 48-well cell culture plates. After incubated for 6, 24, and 72 h, the samples were rinsed by Dulbecco's phosphate-buffered saline (DPBS) solution twice and then were stained with calcein acetoxymethyl ester (Calcein, AM) and ethidium homodimer-1 reagents (LIVE/DEAD viability/cytotoxicity assay kit) for 15 min in cell incubator. Finally, gently rinsed with DPBS solution twice, samples were observed by fluorescence microscopy (IX71, Olympus, Japan).

Hemocompatibility: Hemocompatibility evaluation was carried out according to ISO 10993-4:2020. Healthy human blood was added into anticoagulant tube and mixed with saline solution at the volume ration of 4:5. Mg specimens were incubated in 10 mL of saline solution at 37 °C for 30 min previously before adding 0.2 mL of human diluted blood and then incubated for another 60 min. After centrifuging at 3000 rpm for 5 min, the sample supernatant was recorded as optical densities (ODs, 545 nm) by UV–vis spectrophotometer (UH5300, Hitachi, Japan). Normal saline solution was measured as a negative control (ODn) and sterilized distilled water as positive control (ODp). Hemolysis rate was calculated by the following equation

Hemolysis rate(%) =
$$\frac{(OD_s - OD_n)}{(OD_n - OD_n)} \times 100\%$$
 (1)

Platelet Adhesion: The naked Co-Cr, JDBM Mg alloy, PDA, and Cu10 specimens were sterilized with UV for 1 h prior to the assay. The fresh human platelet rich plasma (PRP) obtained from the Huashan Hospital, China was used in this study following ethics standards. First, 1 mL of PRP was placed with each sample and incubated for 1 h at 37 °C. Afterward, the samples were gently rinsed three times with phosphate-buffered saline (PBS) and fixed with 2.5% glutaraldehyde for 2 h at room temperature, followed by dehydration in a gradient ethanol/distilled water mixture (50%, 60%, 70%, 80%, 90%, and 100%) for 5 min in turn, and finally dried. The specimen surfaces were examined by SEM following a thin gold coating.

Nitric Oxide (NO) Release: Cells were cultured for 1 d and then collected supernatant for Griess reagent test (Beyotime). 50 μL of each

Cell Migration and Viability Assay: The extracts of samples were prepared as previously described in Immersion test section for 3 d. On the other hand, the single Mg²⁺ and Cu²⁺ medium groups were also collected according to ICP released during 3 d immersion, which placed on the bottom chamber of 96-well transwell plates. Cells were cultured on upper compartment of transwell plates with density of 1×10^4 cells mL⁻¹ in 100 µL of each culture medium for 48 h attachment. After fixed by 4% paraformaldehyde solution for 10 min, rinsed by distilled water for three times, crystal violet staining was conducted to evaluate cell migration. In cell viability assay, cells were cultured on 96-well plates with density of $2\times 10^4~\text{cells}~\text{mL}^{-1}$ in 100 μL of DMEM medium for 24 h attachment. Then, the medium was replaced by extracts solution with 10% fetal bovine serum (FBS) and continuously cultured for 1, 3, and 5 d, respectively. Afterward, adding 10 μL cell counting kit (CCK-8, Beyotime Biotechnology, China) solution to each well and incubated for 2 h in a cell incubator, the OD value was evaluated at 450 nm by microplate reader (iMARK, Bio-Rad, USA).

In Vivo Stent Implantation: JDBM stent with inner diameter (2.08 mm) and outer diameter (2.4 mm) was also pretreated in HF solution for 8 h and then coated with Cu10 coating. JDBM stents, mounted on the balloon catheter delivery system (SINOMED, China) were implanted into abdominal aorta of New Zealand white rabbits (weight 2.2–2.5 kg) under digital subtraction angiography (INNOVA2100, GE, USA). After 1 and 3 months' postimplantation, OCT (LightLab Imaging, United States), DSA (Allura FD10, the Netherlands) and IVUS (GE Vingmed Ultrasound, China) were conducted to examine integrity and efficacy of JDBM stents. All animal experimental procedures were conducted in accordance with guidelines approved by the Animal Research Committee of the Huashan Hospital, Fudan University (approval number: 20171059A004), following the National Institutes of Health guide for the care and use of Laboratory Animals.

Re-Endothelialization Observation: After implantation for 2 weeks, 1 month, and 3 months, stented arteries were perfused by saline solution to remove blood. After immersion fixation in formalin solution for 48 h at 4 $^{\circ}\text{C}$, samples were dehydrated by graded ethanol. Using critical point dried (Leica EM CPD300, Germany) in auto mode for final sample dried and bisected longitudinally for SEM observation. For CD31 (platelet endothelial cell adhesion molecule-1) immunofluorescence staining, samples were treated in the following steps: immersed in 10% formalin solution for 20 h fixation, cut in longitudinally and rinsed by DPBS solution three times, blocked by 1% bovine serum albumin (Sigma-Aldrich, USA) in DPBS solution for 1 h, incubated in mouse monoclonalanti-CD31 antibody (Catalogue No. ab199012, Abcam, England) at 4 °C overnight, incubated by donkey antimouse second antibody (Catalogue No. ab150105, Abcam, England) at 37 °C for 2 h after washed by DPBS solution three times. Fluorescence images were obtained by an inverted microscope (DM2500, Leica, Germany).

XRM and HE Staining: In vivo stented arteries were harvested and evaluated by XRM (radia 520 Versa, Zeiss, Germany) after 1 and 3 months' implantation. XRM is a high resolution of computed tomography (CT) with highest spatial resolution of 0.7 μ m. After harvested from 1 and 3 months, stents were fixated, dehydrated, embedded, sealed, and sliced in sequence. HE staining was taken to assess inflammation responses of vascular tissues that surrounded the stent during re-endothelialization process. Histological images were captured with an inverted microscope (DM2500, Leica, Germany).

RNA-seq: Total RNA was isolated with TRIzol (Invitrogen) from cells. Standard illumine HiSeq2000 sequencing was applied in Sequencing. P < 0.05 and Fold-change > 1.5 or Fold-change < -1.5 were set as filter conditions of differentially expressed genes (DEGs). The GO analysis and KEGG pathway analysis were performed by R software based on DAVID website tool.

Western Blotting Analysis: The total proteins of cells were extracted via radio-immunoprecipitation assay (RIPA) lysis buffer and determined by bicinchoninic acid (BCA) protein assay kit (Thermo Fisher Scientific,



www.afm-journal.de

Waltham, MA, USA). The proteins were separated using 10% sodium dodecyl sulfate polyacrylamide gel electrophoresis (SDS-PAGE) gels and transferred to poly(vinylidene fluoride) (PVDF) membranes (0.45 mm, Solarbio, Beijing, China). The membranes were blocked with 5% nonfat milk for 1 h at room temperature and then incubated with primary antibodies at 4 °C for 12 h. The following antibodies were tested: NLRP3, IL-1 β (1:1000, Abcam, UK) rabbit polyclonal antibodies. The α -tubulin rabbit polyclonal antibody (1:4000, Proteintech Group. Inc) was used as loading controls. The secondary antibodies were antimouse or antirabbit antibody and conjugated to horseradish peroxidase (1:4000, Proteintech Group. Inc). The secondary antibodies were used at a 1:4000 dilutions and were incubated for \approx 1 h at room temperature. The bands were visualized with electrochemiluminescence (ECL) reagents (Thermo Fisher Scientific) and developed by Omega Lum G (Aplegen, USA).

ELISA Assay: The concentration of EGF in cell culture medium was measured by a commercial ELISA kit (R&D Systems). In brief, a specific anti-EGF monoclonal antibody was coated onto a microplate. Standards and samples were added to microplate. EGF was detected with biotinylated goat anti-EGF antibody and peroxidase-conjugated streptavidin. Peroxidase substrate was added and the reaction stopped using Stop solution. Absorbance was measured at 450 nm and absolute protein levels were interpolated from the standard curve.

Statistics and Data Analysis: Parallel experiments were conducted at least in triplicate for statistical significance. The data were expressed as means \pm standard error. Statistical analysis was performed by GraphPad Prism software using one-way analysis of variance (ANOVA) with Tukey post hoc test or two-tailed unpaired Student's t-test. Differences were considered significant at (*) p < 0.05, (*) p < 0.05, (**) p < 0.01, (***) p < 0.01, (***) p < 0.01, (***)

Supporting Information

Supporting Information is available from the Wiley Online Library or from the author.

Acknowledgements

The authors would like to thank the National Natural Science Foundation of China (Nos. U1804251, 51701041, and 51971141) and the Program for Medical Key Department of Shanghai (ZK2019A10). The authors thank MicroPort Scientific Corporation for providing Co–Cr stents, Prof. Wen Li from Shanghai University for her careful guidance on QCM-D, and Chao Xing from Shanghai Jiao Tong University for his help on 3d figure modeling.

Conflict of Interest

The authors declare no conflict of interest.

Data Availability Statement

The data that support the findings of this study are available from the corresponding author upon reasonable request.

Keywords

biodegradable Mg alloys, bioresorbable cardiovascular stents, coppereluting coatings, corrosion-resistance, re-endothelialization

Received: May 17, 2022 Revised: July 18, 2022 Published online:

- [1] R. Piccolo, K. H. Bonaa, O. Efthimiou, O. Varenne, A. Baldo, P. Urban, C. Kaiser, W. Remkes, L. Räber, A. de Belder, A. W. J. van't Hof, G. Stankovic, P. A. Lemos, T. Wilsgaard, J. Reifart, A. E. Rodriguez, E. E. Ribeiro, P. W. J. C. Serruys, A. Abizaid, M. Sabaté, R. A. Byrne, J. M. de la Torre Hernandez, W. Wijns, P. Jüni, S. Windecker, M. Valgimigli, Lancet 2019, 393, 2503.
- [2] I. Cockerill, C. W. See, M. L. Young, Y. Wang, D. Zhu, Adv. Funct. Mater. 2020, n/a, 2005361.
- [3] H. Mori, D. R. Atmakuri, S. Torii, R. Braumann, S. Smith, H. Jinnouchi, A. Gupta, E. Harari, M. Shkullaku, R. Kutys, D. Fowler, M. Romero, R. Virmani, A. V. Finn, J. Am. Heart Assoc. 2017, 6, e007244.
- [4] Z. Yang, Y. Yang, L. Zhang, K. Xiong, X. Li, F. Zhang, J. Wang, X. Zhao, N. Huang, Biomaterials. 2018, 178, 1.
- [5] S. Jin, L. Ren, K. Yang, J. Mater. Sci. Technol. 2016, 32, 835.
- [6] Y. Liu, Y. Zheng, X.-H. Chen, J.-A. Yang, H. Pan, D. Chen, L. Wang, J. Zhang, D. Zhu, S. Wu, K. W. K. Yeung, R.-C. Zeng, Y. Han, S. Guan, Adv. Funct. Mater. 2019, 29, 1805402.
- [7] R. M. Touyz, Am. J. Physiol.: Heart Circ. Physiol. 2008, 294, H1103.
- [8] C. Chen, J. Chen, W. Wu, Y. Shi, L. Jin, L. Petrini, L. Shen, G. Yuan, W. Ding, J. Ge, E. R. Edelman, F. Migliavacca, *Biomaterials* 2019, 221, 119414.
- [9] B. S. P. K. Kandala, G. Zhang, C. Lcorriveau, M. Paquin, M. Chagnon, D. Begun, V. Shanov, *Bioact. Mater.* 2021, 6, 1663.
- [10] R. Waksman, R. Pakala, P. K. Kuchulakanti, R. Baffour, D. Hellinga, R. Seabron, F. O. Tio, E. Wittchow, S. Hartwig, C. Harder, R. Rohde, B. Heublein, A. Andreae, K.-H. Waldmann, A. Haverich, *Catheter. Cardiovasc. Interventions* 2006, 68, 607.
- [11] J. Liu, B. Zheng, P. Wang, X. Wang, B. Zhang, Q. Shi, T. Xi, M. Chen, S. Guan, ACS Appl. Mater. Interfaces 2016, 8, 17842.
- [12] H. Hornberger, S. Virtanen, A. R. Boccaccini, Acta Biomater. 2012, 8, 2442.
- [13] L. Mao, L. Shen, J. Chen, Y. Wu, M. Kwak, Y. Lu, Q. Xue, J. Pei, L. Zhang, G. Yuan, R. Fan, J. Ge, W. Ding, ACS Appl. Mater. Interfaces 2015, 7, 5320.
- [14] L. Y. Li, L. Y. Cui, R. C. Zeng, S. Q. Li, X. B. Chen, Y. F. Zheng, M. B. Kannan, Acta Biomater. 2018, 79, 23.
- [15] J. S. Lee, P. Han, E. Song, D. Kim, H. Lee, M. Labowsky, J. Taavitsainen, S. Ylä-Herttuala, J. Hytönen, M. Gülcher, K. Perampaladas, A. J. Sinusas, J. Martin, A. Mathur, T. M. Fahmy, Nano Lett. 2018, 18, 272.
- [16] M. F. Brancati, F. Burzotta, C. Trani, O. Leonzi, C. Cuccia, F. Crea, Pragmatic Obs. Res. 2017, 8, 137.
- [17] R. Busch, A. Strohbach, S. Rethfeldt, S. Walz, M. Busch, S. Petersen, S. Felix, K. Sternberg, Acta Biomater. 2014, 10, 688.
- [18] C. Zhang, Y. Ou, W.-X. Lei, L.-S. Wan, J. Ji, Z.-K. Xu, Angew. Chem., Int. Ed. 2016, 55, 3054.
- [19] F. Zhang, Q. Zhang, X. Li, N. Huang, X. Zhao, Z. Yang, Biomaterials 2019, 194, 117.
- [20] H. Yu, H. Qiu, W. Ma, M. F. Maitz, Q. Tu, K. Xiong, J. Chen, N. Huang, Z. Yang, Small 2021, 17, 2100729.
- [21] X. Liu, Z. Zhen, J. Liu, T. Xi, Y. Zheng, S. Guan, Y. Zheng, Y. Cheng, J. Mater. Sci. Technol. 2015, 31, 733.
- [22] C. Xu, Y. Shan, M. Bilal, B. Xu, L. Cao, Q. Huang, Chem. Eng. J. 2020, 395, 125093.
- [23] L. Fabbrizzi, F. Foti, S. Patroni, P. Pallavicini, A. Taglietti, Angew. Chem., Int. Ed. Engl. 2004, 43, 5073.
- [24] M. Ghosh, S. Mandal, A. Roy, S. Chakrabarty, G. Chakrabarti, S. K. Pradhan, *Mater. Sci. Eng.*, C 2020, 106, 110160.
- [25] H. Pan, K. Pang, F. Cui, F. Ge, C. Man, X. Wang, Z. Cui, Corros. Sci. 2019, 157, 420.
- [26] K. Zhou, Y. Li, L. Zhang, L. Jin, F. Yuan, J. Tan, G. Yuan, J. Pei, Bioact. Mater. 2021, 6, 262.
- [27] F. Gao, Y. Hu, G. Li, S. Liu, L. Quan, Z. Yang, Y. Wei, C. Pan, Bioact. Mater. 2020, 5, 611.





www.afm-journal.de

- ·
- [28] L.-C. Zhang, M. Xu, Y.-D. Hu, F. Gao, T. Gong, T. Liu, X. Li, C.-J. Pan, Appl. Surf. Sci. 2018, 451, 20.
- [29] H. Li, F. Peng, D. Wang, Y. Qiao, D. Xu, X. Liu, Biomater. Sci. 2018, 6, 1846.
- [30] N. Lyu, Z. Du, H. Qiu, P. Gao, Q. Yao, K. Xiong, Q. Tu, X. Li, B. Chen, M. Wang, G. Pan, N. Huang, Z. Yang, Adv. Sci. 2020, 7, 2002330.
- [31] Q. Liu, S. Zheng, K. Ye, J. He, Y. Shen, S. Cui, J. Huang, Y. Gu, J. Ding, Biomaterials 2020, 263, 120327.
- [32] M. Gueguen, Z. Keuylian, V. Mateo, N. Mougenot, A.-M. Lompré, J.-B. Michel, O. Meilhac, L. Lipskaia, I. Limon, J. Pathol. 2010, 221, 331.
- [33] A. W. Carpenter, M. H. Schoenfisch, Chem. Soc. Rev. 2012, 41, 3742.
- [34] R. H. Adams, K. Alitalo, Nat. Rev. Mol. Cell Biol. 2007, 8, 464.
- [35] M. T. Holderfield, C. C. Hughes, Circ. Res. 2008, 102, 637.

- [36] V. A. Rathinam, K. A. Fitzgerald, Cell 2016, 165, 792.
- [37] Y. Dautova, A. N. Kapustin, K. Pappert, M. Epple, H. Okkenhaug, S. J. Cook, C. M. Shanahan, M. D. Bootman, D. Proudfoot, J. Mol. Cell. Cardiol. 2018, 115, 82.
- [38] M. Wortmann, E. Skorubskaya, A. S. Peters, M. Hakimi, D. Böckler, S. Dihlmann, Biophys. Res. Commun. 2019, 511, 343.
- [39] O. R. Lindberg, A. Brederlau, H. G. Kuhn, Stem Cell Rep. 2014, 2, 440.
- [40] K. P. Koster, R. Thomas, A. W. J. Morris, L. M. Tai, J. Cereb, Blood Flow Metab. 2016, 36, 1865.
- [41] L. Huang, F. Wang, Y. Wang, Q. Cao, T. Sang, F. Liu, S. Chen, PLoS One 2015, 10, e0129665.
- [42] H. Elamaa, M. Kihlström, E. Kapiainen, M. Kaakinen, I. Miinalainen, S. Ragauskas, M. Cerrada-Gimenez, S. Mering, M. Nätynki, L. Eklund, eLife 2018, 7, e37776.